

Advances in freeform optical metrology using a multibeam low-coherence optical probe (Quad-Probe)

Christopher J. Ditchman, Damon W. Diehl, Christopher T. Cotton, Nathan E. Burdick, David Woodlock, Jun Zou

ASE Optics, LLC, a wholly owned subsidiary of Rochester Precision Optics, LLC
850 John St., West Henrietta NY 14586, USA

ABSTRACT

Conformal windows reduce drag, but introduce optical aberrations. Corrector optics minimize such optical aberrations, but they feature complex surfaces that cannot presently be measured interferometrically. To address this problem, ASE Optics has developed a non-contact "Quad-Probe" that measure the position and orientation of surfaces. By scanning the probe over the surface of the optic, a 3D model of the interior and exterior surfaces can be built. Furthermore, the Quad-Probe can be used inside a polishing machine, and feedback from the Quad-Probe can be used to guide the scanner in measuring an unknown part.

Keywords: surface metrology, optical metrology, freeform optics, conformal optics, aspheric optics, low-coherence interferometry, blind contouring

1. INTRODUCTION

The commercial availability of deterministic polishing systems has given optical designers greater freedom to design optical elements that differ significantly from spherical.^{1,2} This in turn has spurred the need for improved metrology solutions for freeform surfaces.³ The ideal metrology solution would simultaneously measure interior and exterior surfaces to sub-micron accuracy and be adaptable to various shapes and sizes without requiring the interchange of expensive reference optics.

To address this need, ASE Optics, LLC has developed a multi-point non-contact optical probe that uses low-coherence dual wavelength interferometry to measure both the position and orientation of a surface with respect to the probe. Scanning the probe in a free-form manner over the object yields a three dimensional model of the object. Of particular interest is a proposed arch-shaped lens to be used to correct optical aberrations introduced by aerodynamic ogive domes.⁴ A conceptual drawing of the arch optic is shown in Figure 1. The two key metrology challenges for the arch optic are that the interior and exterior surfaces may not be spherical, and the interior and interior surfaces may not be parallel to one another.

The Lumetrics OptiGauge is a fiber-based low-coherence interferometer that can simultaneously measure the optical thicknesses of all layers within a multilayer material. The technology was invented at the Eastman Kodak Company and commercialized by Lumetrics, Inc.^{5,6} The OptiGauge interferometer emits broadband infrared light centered at 1.3 μm . The interferometer can measure layers with optical thickness as thin as 12 μm and as thick as 12 mm with a resolution of 0.1 μm .

The Quad-Probe is a new probe for the OptiGauge.⁷ Instead of a single beam, it projects four beams in a square pattern. This is shown conceptually in Figure 2 (a). The principles of operation of the Quad-Probe have been previously published⁷ but are reviewed in brief below.

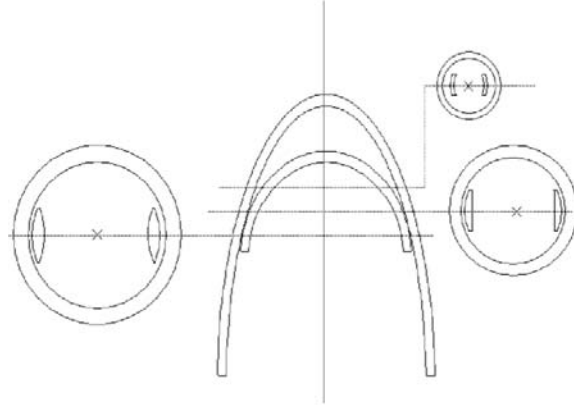


Figure 1: A conformal dome with an aspheric arch corrector optic are two freeform shapes that can be measured using a Quad-Probe in conjunction with a five axis scanning system.⁴

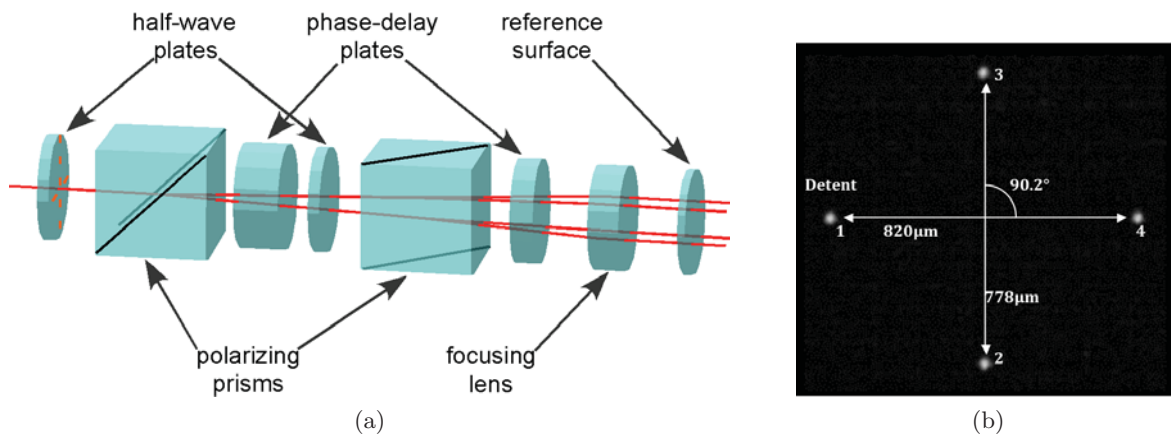


Figure 2: (a) Illustration of the Quad-Probe components (not to scale) and (b) photograph of the Quad-Probe spot pattern. Precise spot positions are used to create accurate models of the surface geometry

2. METHODS AND PROCEDURES

2.1 Principles of Quad-Probe Operation

An illustration of the interior components of the Quad-Probe is shown in Figure 2 (a). The Quad-Probe splits the OptiGauge measurement beam into four beams that are separated in both space and phase. The key components of the Quad Probe are a pair of half-wave plates, a pair of Wollaston polarizing prisms, and a pair of birefringent phase-delay plates. The first half-wave plate is used to rotate the incoming beam polarization to 45° with respect to the first polarizing prism's axes. The first polarizing prism vertically splits the incident beam into two orthogonally polarized beams with equal intensity. The two beams then pass through a calcite crystal aligned so that one polarization is delayed by 1.2 mm with respect to the other. Subsequently, a second half-wave plate rotates the polarizations by 45° . The second polarizing prism splits each of the beams horizontally into two beams, resulting in four beams. A thinner calcite phase plate creates a phase delay of 0.6 mm between the polarizations. The result is a phase separation of approximately $600 \mu\text{m}$ between each beam. A final lens focuses the beams to create a square pattern within the focal region. A photograph of the square spot pattern appears in Figure 2 (b). The diagonals across the pattern are $820 \mu\text{m}$ and $778 \mu\text{m}$. The angle between the diagonals is 90.2° . Figure 3 shows the OptiGauge waveform for a single Quad-Probe measurement of a piece of glass 3.7 mm thick. The distances between corresponding peaks on each surface establish the geometry of the first surface relative to the reference plate and the position of the second surface relative to the first. Each set of four

Further author information:

C.J.D.: E-mail: chrisd@aseoptics.com, Telephone: 1 585 355 0993

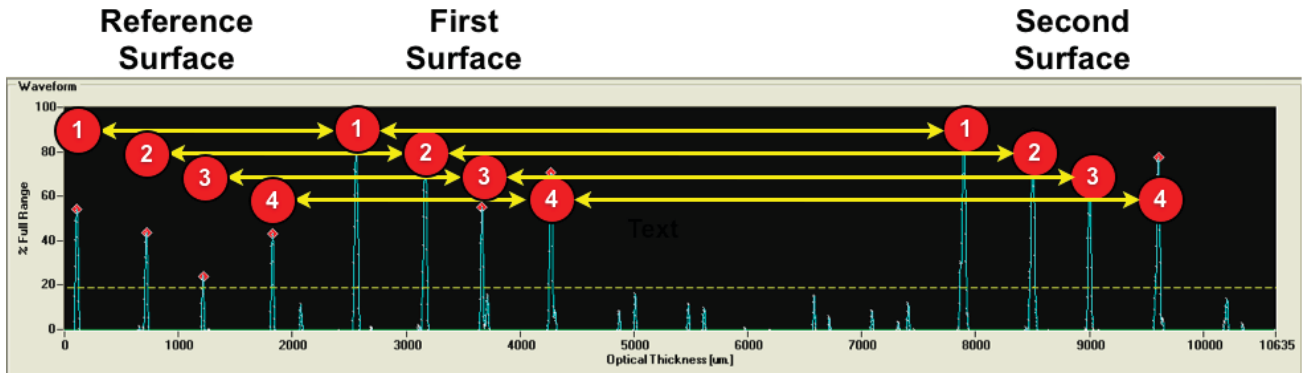


Figure 3: Quad-Probe OptiGauge waveform showing the quadruple peaks for each surface. The location of surface peaks relative to the reference peaks provides the means for constructing a 3-D model of the measured surfaces.

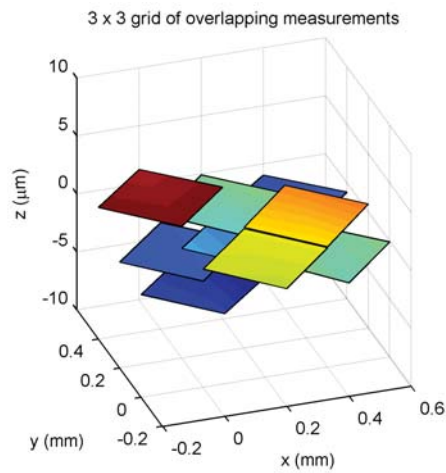


Figure 4: Isometric view of nine overlapping measurement facets illustrates how a surface is constructed by measuring a series of locations.

measurements creates a square polygon that we term a "measurement facet." We build up a three-dimensional model of surfaces using Quad-Probe measurements at different locations on the part. Figure 4 illustrates a small grid of overlapping facets.

2.2 Quad-Probe Scanning Systems

Our metrology system consists of the following four key components: a four-beam Quad-Probe, a Lumetrics OptiGauge, and a computer (for motion control, data acquisition, and data analysis), and a five-axis freeform scanning system. These are shown in Figure 5. We have completed construction of a testbed five-axis scanner, consisting of three linear stages in the x-, y-, and z-directions and two rotation axes about the y- and z-axes. (See component (d) in Figure 5.) This system is capable of measuring freeform optics. The spot pattern for the current Quad-Probe prototype (component (a) in Figure 5) is shown in Figure 2 (b). The beams are parallel to within 0.1 microradians. The geometry of the spot pattern is used to increase accuracy during reconstruction of the measured optic's surfaces. The Quad-Probe offers three advantages over a single-beam probe; it can measure both position and orientation of the surface, correct for refraction at the surface, and improve statistical uncertainty by overlapping measurements. By simultaneously measuring four points on a surface, we are able to determine both the position and the orientation of the measured region with respect to the probe. The measurements from the four beams create a four cornered polygon termed a "facet." We have previously

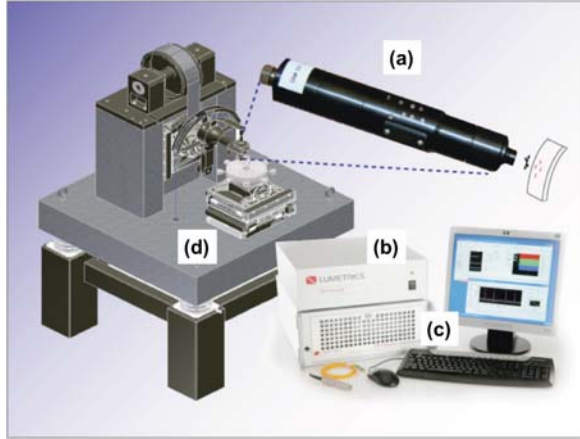
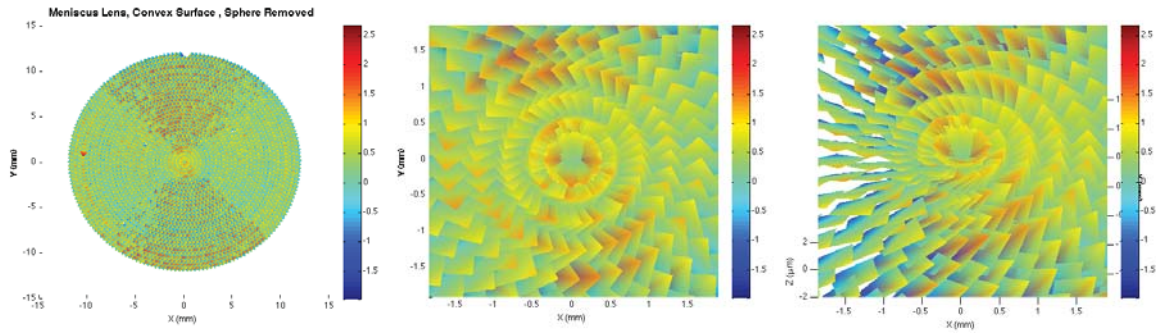


Figure 5: Components of the Quad-Probe freeform metrology system including a Quad-Probe, a Lumetrics OptiGauge, a computer, and a five-axis scanning system.



(a) Convex surface of meniscus lens (b) Zoom of center region (c) Small rotation of center region

Figure 6: The convex surface of a measured positive meniscus lens in (a) shows evidence of probe tilt with respect to the surface during the course of the scan. Examining the central region of the surface more closely in (b) and (c) reveals tilted facets which can be corrected in post processing.

published research that demonstrated the Quad-Probe can construct accurate three-dimensional models of the interior and exterior surfaces of planar and spherical objects.⁷ The spacing between measurements is generally chosen so that the facets overlap. This creates measurement redundancy that can be useful for detecting (and sometimes correcting) mechanically-induced measurement errors. An example of overlapping facets is shown in Figure 4. Figure 6 zooms in on a central region of data to show facet tilt due to misalignment that can be corrected with post-processing techniques.

When we measure an object, such as a lens, we construct 3-D models of the surfaces by calculating the positions on the first surface and then project down to construct the interior surface. If the probe is tilted with respect to the exterior surface of an optic, then the measured distance to the interior surface is shorter due to refraction at the air-glass interface. If refraction is not accounted for and the propagation angle is not adjusted, it leads to position error in the second surface. As an example, consider scanning a probe across a plano-convex lens while maintaining the probe normal to the interior planar surface. The measurement of the exterior surface may be correct, but closer inspection reveals that the measurement of the interior surface is distorted. This error is demonstrated via simulation in Figure 7. The error is small near the center of the lens where the probe is nearly normal to both lens surfaces but increases further from center if we project along an uncorrected probe pointing. The position and orientation information from a facet at an interface, combined with the refractive index on each side of the interface, are sufficient to calculate and account for refraction effects. If the refractive index is not known, it can be measured using the OptiGauge. Figure 8 (a) shows the difference between actual and measured thickness as the angle of incidence is increased, for a variety of thicknesses of fused silica. From this

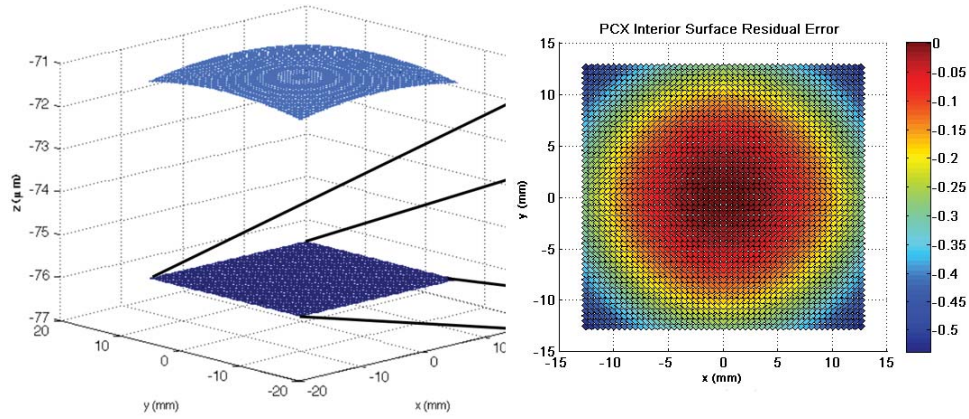


Figure 7: A probe is simulated being scanned across a plano-convex lens while maintaining the probe's normal to the interior planar surface. If refraction is not accounted for at the exterior interface, measurable distortions occur during the construction of the interior surface.

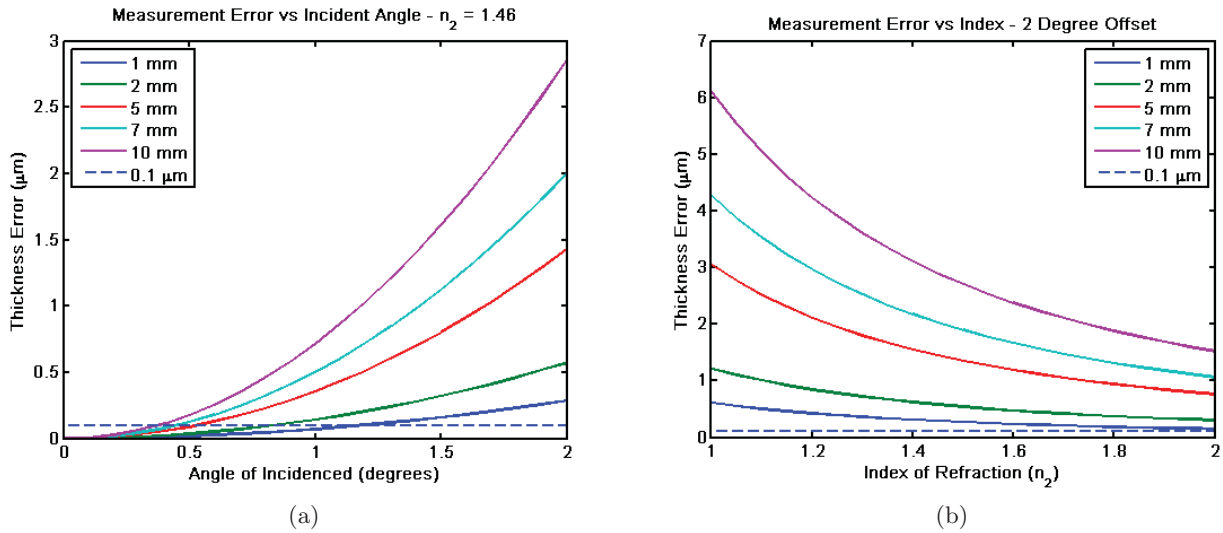
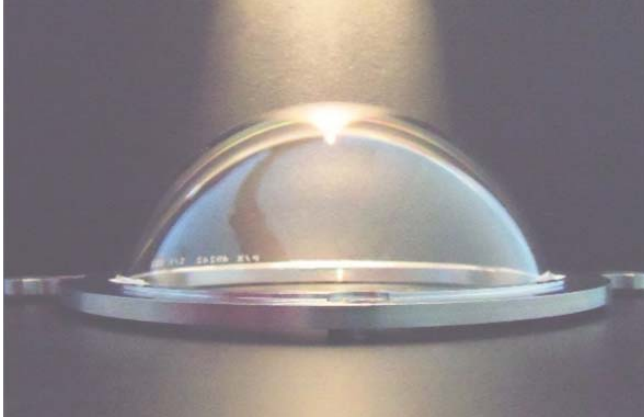
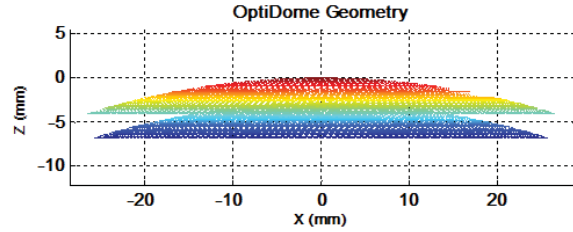


Figure 8: The expected measurement error at an air-glass interface when refraction is not accounted for is shown for a number of measured thicknesses. At a fixed index there is a threshold angle at which the error becomes larger than the minimum measurable difference of $0.1 \mu\text{m}$ (a). When we hold the probe at an angle of 2° , all of the sample thicknesses have measurable errors above the minimum threshold for materials whose refractive index range between 1 and 2.



(a) OptiDome



(b) Measured OptiDome surface geometry

Figure 9: We borrowed and measured an Optimax Systems OptiDome (S/N 002) using an ASE Optics Quad Probe in conjunction with OptiPro’s UltraSurf measurement platform. The OptiDome (a) has a clear aperture of 164.64 mm. The measured surface geometry (b) is fit to a best fit sphere and returns values of 88.84 mm for the exterior radius, 85.96 mm for the interior surface radius. The interior surface is decentered from the exterior surface by $-0.28 \mu\text{m}$ in x , $1.04 \mu\text{m}$ in y , and $-0.57 \mu\text{m}$ in z .

we can see that the measurement error increases with both sample thickness and angle of incidence. Figure 8 (b) shows the measurement error for a beam at 2° angle of incidence as a function of index of refraction, again for a variety of thicknesses. From this we see that measurement error decreases with index of refraction. This is because the higher index of refraction pulls the beam toward the normal direction within the medium.

The major conclusion to draw from this experiment is that, in general, the effects of refraction at the surface interfaces should not be neglected. This will be an advantage for the Quad-Probe over the conventional OptiGauge probe, because the Quad-Probe measures the orientation of the surface with respect to the probe.

3. RESULTS AND DISCUSSION

3.1 OptiDome Measurement

Optimax Systems created a series of six-inch diameter concentric F/0.53 spherical fused silica domes. These OptiDomes to serve as a measurement standard for organizations that are developing metrology systems for large format freeform optics.⁸ The dome has a nominal outside radius of 88.9 mm, a clear aperture of 164.64 mm and a wall thickness of 2.9 mm. Some of the domes have been created with intentional errors. We borrowed an OptiDome with the serial number 002 from Optimax (pictured in Figure 9) and measured the dome using an ASE Optics Quad Probe in conjunction with OptiPro’s UltraSurf system. The UltraSurf scanned the OptiDome by measuring concentric lines of latitude on the dome while maintaining a constant distance to the exterior surface. The Quad-Probe simultaneously recorded distances to the exterior and interior surfaces at four locations, a *facet*, relative to a reference plate at the tip of the Quad-Probe. We measured a 100 mm diameter area around the center of the dome so that we could compare our results with a Zygo interferometer. We applied the processes described in Section 2.2 to detect and correct for facet tilt due to probe misalignment as well as account for refraction when reconstructing the interior surface.

The surfaces in Figure 9 (b) were each fit to a best fit sphere where we calculated the convex (Figure 10 (a)) surface to have a 88.84 mm radius of curvature and the concave (Figure 10 (b)) surface to have a 85.96 mm radius of curvature. The center of curvature of the two surfaces were used to determine that the interior surface is decentered from the exterior surface by $-0.28 \mu\text{m}$ in x , $1.04 \mu\text{m}$ in y , and $-0.57 \mu\text{m}$ in z . The physical thickness map (Figure 10 (c)) shows evidence of decentration between the two surfaces and some astigmatism. The

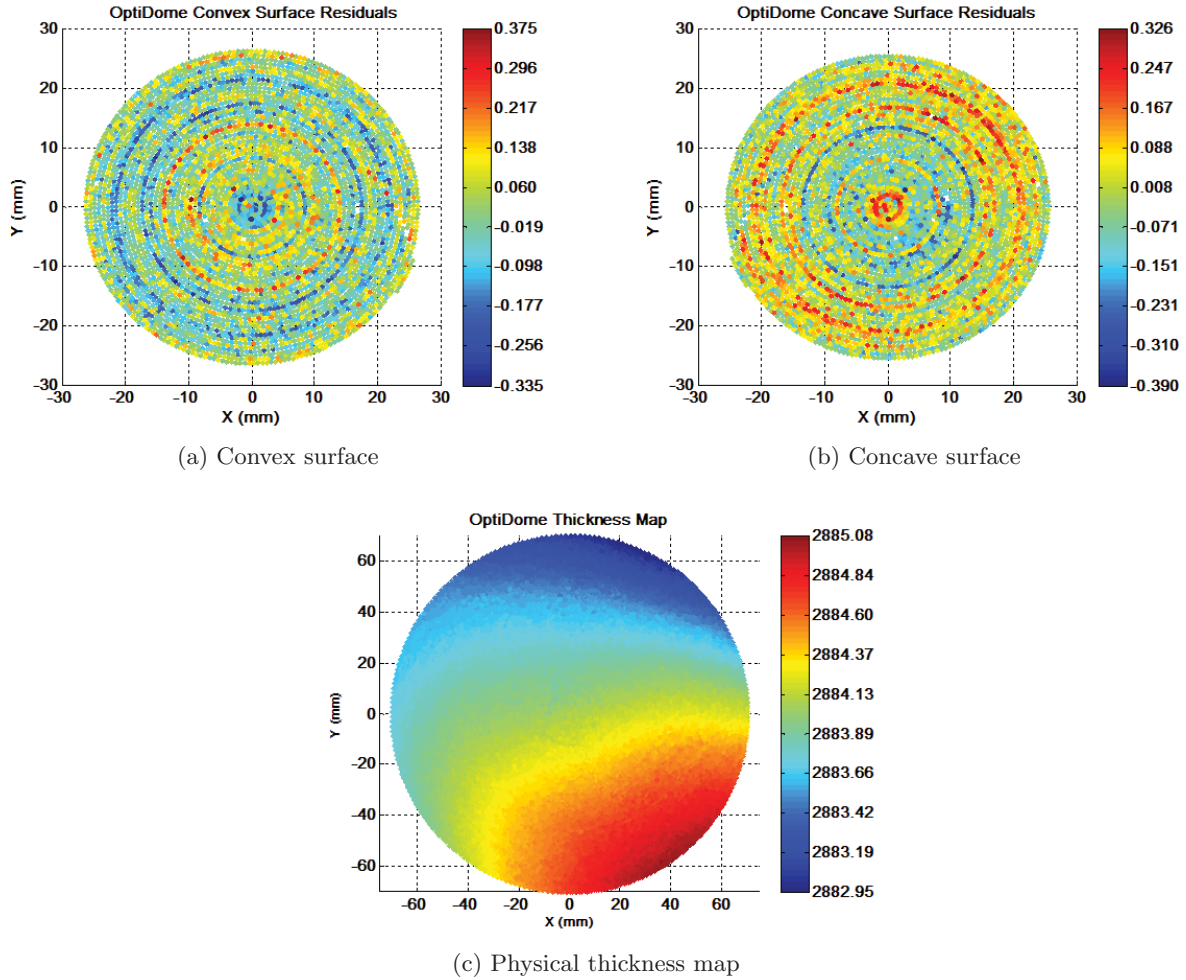


Figure 10: The OptiDome convex surface has a best fit radius of 88.84 mm with the residuals (a) having a standard deviation $\sigma = 0.1 \mu\text{m}$. The concave surface has a best fit radius of 85.96 mm with the residuals (b) having a standard deviation $\sigma = 0.1 \mu\text{m}$. The physical thickness plot (c) shows evidence of decentration between the two surfaces and some astigmatism. Vertical scale units are given in microns.

OptiGauge's noise level has approximately $0.1 \mu\text{m}$ of standard deviation, so the visible artifacts in Figure 10 are likely caused by measurement noise.

We chose our test region on the OptiDome to correspond to an area that we could measure with a Zygo. Results from the Zygo are shown in Figure 11 where tip, tilt, and power have been removed. The residual plots of Figure 10 were compared to the Zygo measurements of Figure 11 which resulted in difference plots shown in Figure 12. The standard deviation of the difference plot for the convex and concave surfaces are each $0.1 \mu\text{m}$. The comparisons are constrained by the measurement accuracy of the scanning system. With averaging and other processing techniques it is possible to further improve the accuracy of the system. The rings that appear in the data are probably due to a time varying drift in the measurement system.

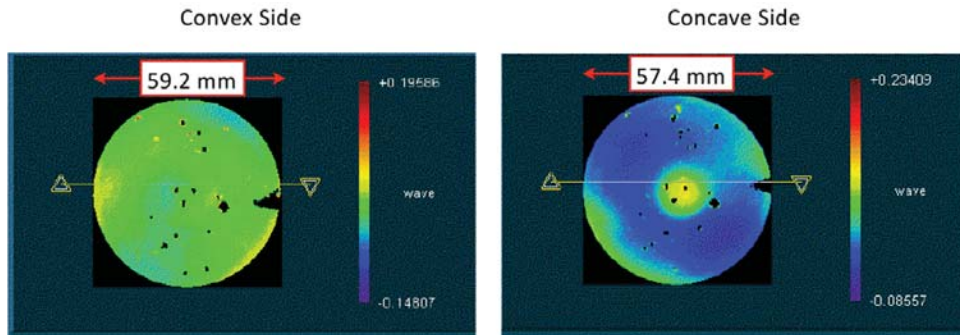
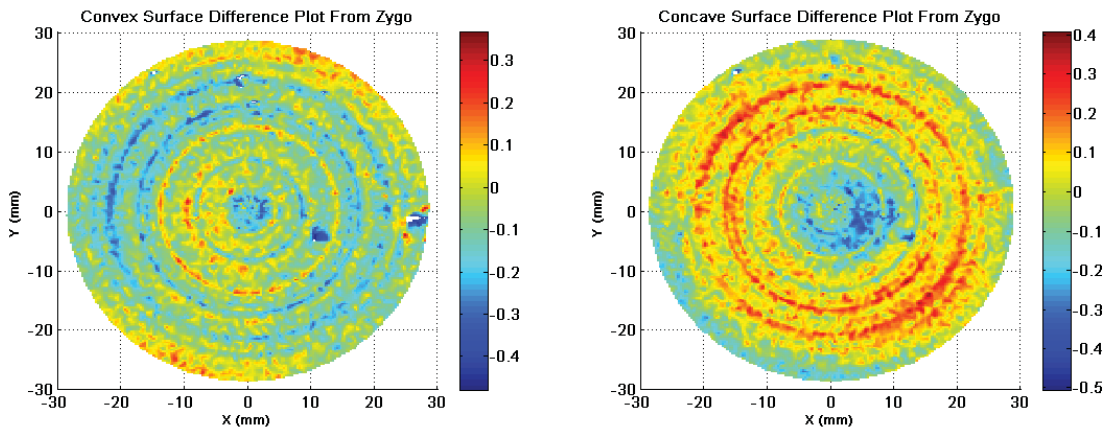


Figure 11: Zygo measurement of the OptiDome convex and concave surface variation in the same region measured using the Quad-Probe and UltraSurf. A center slice across the convex surface exhibits deviations of 0.344 waves PV and 0.015 waves rms with 0.023 waves of power and the concave side slice exhibits deviations of 0.320 waves PV and 0.029 waves rms with 0.387 waves of power.



(a) Convex surface

(b) Concave surface

Figure 12: The OptiDome Quad-Probe measurement is compared to a Zygo measurement of the same area for the convex (a) and concave (b) surfaces. The standard deviation of the differences on each plot $0.1 \mu\text{m}$ corresponds to the system's measurement accuracy at the time of the scan.

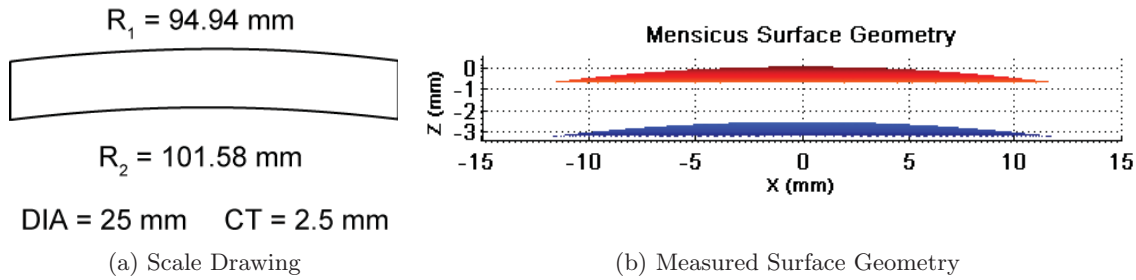


Figure 13: The measured meniscus lens is specified (a) to have a convex surface radius of 94.94 mm and a concave radius of 101.58 mm. The scanning system results (b) returned a convex surface radius of 94.988 ± 0.005 mm and a concave surface radius 101.307 ± 0.005 mm.

3.2 Meniscus Lens Measurement

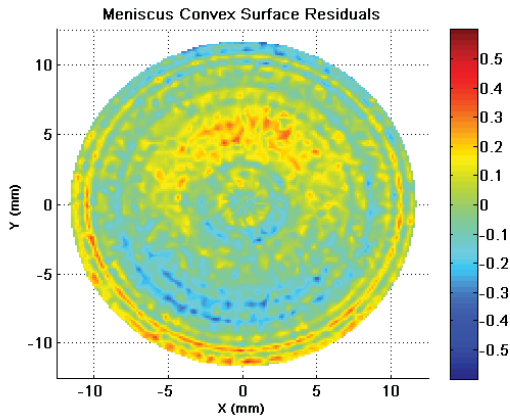
A key advantage of the Quad-Probe lies in its ability to simultaneously measure two non-parallel surfaces. To demonstrate the scanner’s ability to measure non-concentric surfaces on a more conventional optic, we measured a 25 mm diameter positive meniscus lens with an outer radius of 94.94 mm and an interior radius of 101.58 mm using the Quad-Probe on OptiPro’s UltraSurf measurement platform. A scale drawing of the lens cross section appears in Figure 13 (a). Three-dimensional models of the measured meniscus surface geometry are shown in Figure 13 (b).

We measured the meniscus lens surfaces using our Zygo interferometer. Images of these measurements, after removal of tip, tilt and defocus are shown in Figures 14 (c) and 14 (d). The Zygo measured the radii of curvature to be 94.81 ± 0.02 mm for the convex surface and 101.12 ± 0.06 mm for the concave surface. The surfaces constructed using Quad-Probe data were each fit to a best fit sphere and were then subsequently fit to remove tip, tilt, and defocus to compare with the Zygo data. The best fit spheres give a convex surface radius of 94.988 ± 0.005 mm and a concave surface radius of 101.307 ± 0.005 mm. Plots of the surface residuals and difference with the Zygo data are shown in Figure 14. The standard deviation of the residuals after removing the best fit sphere is $0.14 \mu\text{m}$ for the convex surface and $0.16 \mu\text{m}$ for the concave surface. While the comparison to the Zygo data is limited by the accuracy of the scanning system to about $1 \mu\text{m}$, we were able to measure both interior and exterior surfaces in a single pass without having to disturb the part.

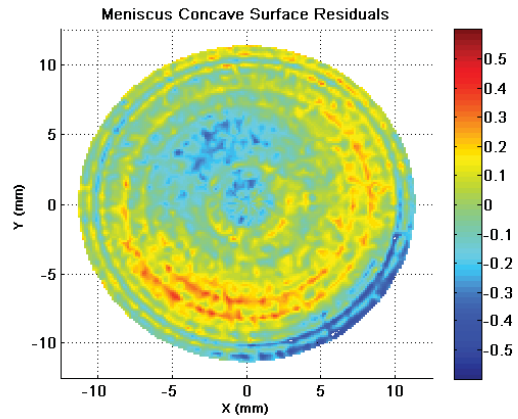
3.3 Blind Contouring Simulation

Because the Quad-Probe measures both the position and orientation of a surface with respect to the probe, we have posited that the Quad-Probe could be used as feedback mechanism to guide the scanner during the measurement of an unknown object. We have termed this metrology approach “blind contouring” in reference to drawing exercises in which the artist traces a complex shape by focusing on local details of position and slope.⁹ To test the feasibility of blind contouring, we have developed a mathematical model of our scanning system using MATLAB. This model allows us to simulate scanning algorithms without risk of damaging an actual probe or object. For a given set of commanded positions of the linear and angular motors, the mathematical model calculates the position and orientation of the Quad-Probe in the local coordinate space of the optic under test. The software then performs a virtual measurement by calculating where each of the four Quad-Probe beams intersects the surface of the virtual object under test. These four virtual measurements can be used to generate a 3-D facet that represents the position and orientation of the surface under test, in the same way that the real Quad-Probe does.

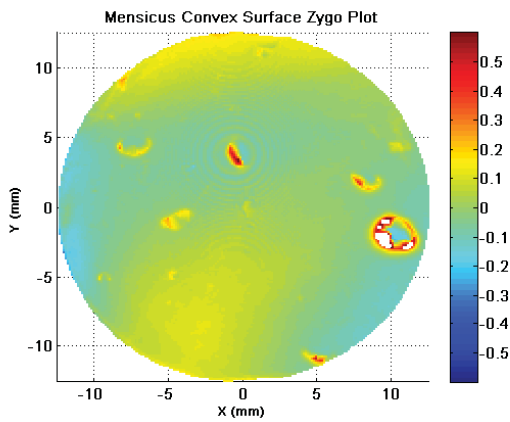
As a first test of blind contouring, we have developed an algorithm that safely “walks” the probe down an unknown convex surface (in this case a paraboloid) without prior knowledge of the surface shape. The algorithm attempts to keep the probe perpendicular to the surface while maintaining a constant, safe separation between the probe and the object. A magnified view of the first few steps of the process is illustrated in Figure 15. The red square at the top of Figure 15 (a) represents the initial location of the face of the probe, and the red



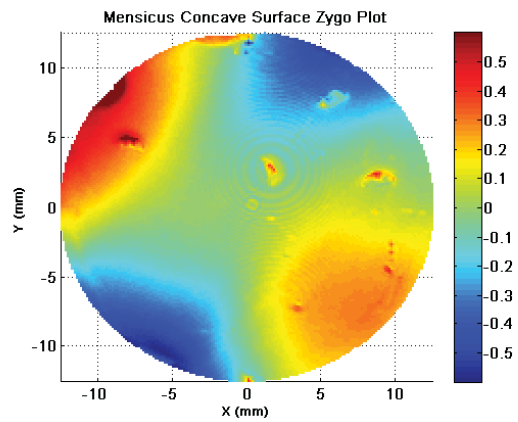
(a) Convex surface Quad-Probe



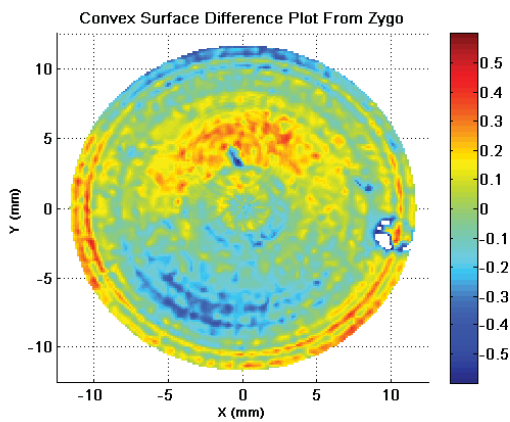
(b) Concave surface Quad-Probe



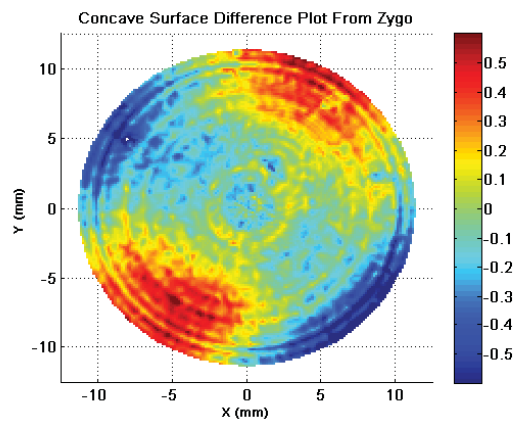
(c) Convex surface Zygo



(d) Concave surface Zygo



(e) Convex surface difference



(f) Concave surface difference

Figure 14: The meniscus lens convex surface has a best fit radius of 94.99 mm with the residuals (a) having a standard deviation $\sigma = 0.14 \mu\text{m}$. The concave surface has a best fit radius of 101.31 mm with the residuals (b) having a standard deviation $\sigma = 0.15 \mu\text{m}$. The Zygo plots of the convex (c) and concave (d) surfaces have some artifacts due to defects in the reference sphere used. The difference between the scanner residuals and Zygo measurement for the convex (e) and concave (f) surfaces are dominated by the accuracy limit of the scanning system. Vertical scale units are given in microns.

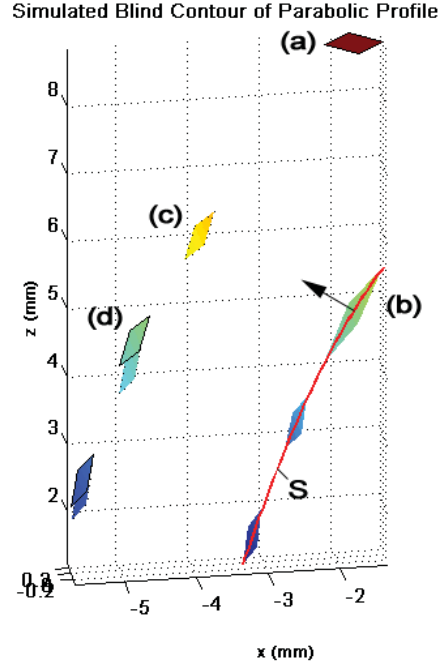


Figure 15: We simulate blind contouring by starting with an initial probe position (a), projecting down to surface S and obtaining a measurement facet (b). The effective facet (c) is where the probe should have been located in order to be normal to the surface. The next blind step location (d) (solid border facet) is calculated relative to the effective measurement facet (c). A new measurement facet is obtained and the process iterates until a stop condition is satisfied.

curve, labeled S , represents the surface being measured. The software first simulates a measurement of the surface by projecting the four Quad-Probe beams and calculating where they intersect the surface. These four measurements create the green facet indicated by (b). Using the position and orientation of the surface facet (b), the software calculates the ideal location of the Quad-Probe, if it were perpendicular to the surface and at the desired safety distance. This is the yellow square indicated by (c). The probe is not actually moved to this location, but it is used as the starting point for the next step of movement. Based on the position and orientation of the ideal probe location (c), the software proposes the next position for the probe. This next position is in the same plane as (c) but one step “down.” This new position is the green facet labeled (d). The probe is moved to this position, and the process starts over again. We have confirmed that the algorithm safely moves the probe down a surface without collision, and stops when either the probe location or the measured facet fall below a pre-set lower threshold for the z -position.

Having successfully developed an algorithm to blind-countour the probe down a line of longitude on an unknown object, we are now developing a similar algorithm for the more complex problem of blind-contouring around a line of latitude. To maintain a fixed line of latitude on a non-rotationally symmetric object, all five stages must be moved, including rotation about the y -axis. This rotation perpendicular to the plane of motion is necessary to keep the probe perpendicular to the surface. The Quad-Probe’s ability to yield information about changes in slope perpendicular to the direction of motion is a critical advantage of the Quad-Probe over a single point probe.

4. FUTURE WORK

We are presently collaborating with OptiPro Systems to incorporate the Quad-Probe into the UltraSurf, a commercial high-precision five-axis scanner.¹⁰ The resulting system will be able to measure complex freeform surface profiles without contacting the surface and with an accuracy limited by the precision of the OptiGauge

and the position accuracy of the scanner. We are additionally collaborating with OptiPro to integrate a Quad-Probe into the UltraForm finishing system.² A Quad-Probe will allow for mid-process checks on the part being polished without removing the part from its mount. This will reduce errors by removing the need to remove and remount the part for testing. The blind contouring algorithms are being adapted for the five axis scanning systems for proof-of-concept testing.

5. CONCLUSIONS

The Quad-Probe offers key advantages in its ability to simultaneously measure position and orientation information. This allows us to detect and correct probe misalignment, correct for refraction effects at interfaces, and use redundancy to improve the accuracy of measurements. The Quad-Probe in conjunction with a five axis scanning system is able to measure large format shapes such as the OptiDome as well as more conventional optics with non-parallel surfaces such as a meniscus lens. Using the UltraSurf platform with the Quad-Probe we have been able to improve our accuracy to about $1\mu\text{m}$ with ongoing efforts to bring the system closer to the measurement limit of $0.1\mu\text{m}$. Future system improvements will focus on implementing and testing the blind contouring algorithm using ASE's testbed five axis systems.

ACKNOWLEDGMENTS

We thank Scott DeFisher, Scott Bambrick, and Mike Bechtold of OptiPro Systems and Rick Plympton and Jessica DeGroot Nelson of Optimax Systems for their continued interest, insights and support during the development and testing of this instrument.

We would like to thank Peter Emmel of ASE Optics for providing Zygo measurements of the OptiDome and meniscus lenses and Wade Cook of ASE Optics for technical assistance.

We gratefully acknowledge the technical assistance from Lumetrics, particularly from Todd Blalock, Filipp Ignatovich, Glen Hallit, and Michael Maher.

The OptiDome sample featured in this paper is generously on loan from Optimax Systems.

REFERENCES

- [1] Jacobs, S. D., Golini, D., Hsu, Y., Puchebner, B. E., Strafford, D., Prokhorov, I. V., Fess, E. M., Pietrowski, D., and Kordonski, W. I., “Magnetorheological finishing: a deterministic process for optics manufacturing,” in [*International Conference on Optical Fabrication and Testing*], Kasai, T., ed., *Proc. SPIE* **2576**, 372–382 (1995).
- [2] Fess, E., Schoen, J., Bechtold, M., Mohring, D., and Bouvier, C., “Ultraform finishing process for optical materials,” in [*Optical Fabrication II: Polishing*], Stahl, H. P., ed., *Proc. SPIE* **5868** (2005).
- [3] in [*Window and Dome Technologies and Materials X*], Tustison, R. W., ed., *Proc. SPIE* **6544** (2007).
- [4] Sparrold, S. W., Knapp, D. J., Manhart, P. K., and Elsberry, K. W., “Capabilities of an arch element for correcting conformal optical domes,” in [*Current Developments in Optical Design and Optical Engineering VIII*], Fischer, R. E. and Smith, W. J., eds., *Proc. SPIE* **3779** (1999).
- [5] Marcus, M. A., “Fiber optic interferometry for industrial process monitoring and control applications,” in [*Fiber Optic Sensor Technology and Applications*], Marcus, M. A. and Culshaw, B., eds., *Proc. SPIE* **4578**, 136–144 (2002).
- [6] Badami, V. G. and Blalock, T., “Uncertainty evaluation of a fiber-based interferometer for the measurement of absolute dimensions,” in [*Recent Developments in Traceable Dimensional Measurements III*], Decker, J. E., ed., *Proc. SPIE* **5879**, 23–41 (2005).
- [7] Diehl, D. W., Ditchman, C. J., and Cotton, C., “Metrology of freeform conformal optics using scanning low-coherence dual-wavelength interferometry,” in [*Window and Dome Technologies and Materials XI*], Tustison, R. W., ed., *Proc. SPIE* **7302** (2009).
- [8] Martucci, M. and Plympton, R., “Round robin testing of the optimax optidome,” in [*Window and Dome Technologies and Materials XI*], Tustison, R. W., ed., *Proc. SPIE* **7302** (2009).
- [9] Edwards, B., [*Drawing on the Right Side of the Brain*], St. Martin’s Press (1979).
- [10] Bambrick, S., Bechtold, M., DeFisher, S., Mohring, D., and Meisenzahl, J., “Recent developments in finishing of deep concave, aspheric, and plano surfaces utilizing the ultraform 5-axes computer controlled system,” in [*Window and Dome Technologies and Materials XI*], Tustison, R. W., ed., *Proc. SPIE* **7302** (2009).